Mixed Percolating Network and Mechanical Properties of Polypropylene/Talc Composites

D. Frihi,[1,2] K. Masenelli-Varlot,[2] G. Vigier,[2] H. Satha[1]

[1]*Laboratoire d'Analyses Industrielles et Génie des Matériaux (LAIGM), Université 08 Mai 1945, Guelma, Algeria*
[2]*Université de Lyon, Institut National des Sciences Appliquées–Lyon, Materials, Engineering, and Sciences (MATEIS), Centre National de la Recherche Scientifique UMR5510, F-69621 Villeurbanne Cedex, France*

Received 7 November 2008; accepted 23 May 2009
DOI 10.1002/app.30890
Published online 28 July 2009 in Wiley InterScience (www.interscience.wiley.com).

ABSTRACT: Injected polypropylene/talc composites were studied to evaluate the conditions leading to the formation of a mixed talc/polymer crystalline lamella percolating network and the influence of such a network on the nanocomposite mechanical properties. The talc was either conventional micrometer-sized (conventional talc) or submicrometer-sized particles (μ-talc). In the case of μ-talc, several talc fractions were studied, ranging from 3 to 30 wt %. The nanocomposite crystallinity was characterized with differential scanning calorimetry and wide-angle X-ray scattering. Talc was found to act as a nucleating agent, and only the α phase was detected. Through quantification on a Wilchinsky diagram, the talc particles were found to lie in the sample plane, the polypropylene crystalline lamellae being orthotropically distributed perpendicularly to the talc particles. The mechanical properties of the composites were tested in different directions by tensile and compression tests. The mechanical behavior of the composites confirmed the microstructural model. For low talc loadings, the composite moduli could not be well fitted by a law of mixtures. The large difference between the observed and predicted moduli was attributed to the formation of a mixed percolating network, including talc particles and polypropylene crystalline lamellae. At high talc loadings, when the mixed percolating network was completely formed, the reinforcement could well be described by parallel coupling, which indicated a classical reinforcement mechanism. Finally, the value of the critical talc fraction, at which the mixed percolating network was formed, was examined as a function of talc. © 2009 Wiley Periodicals, Inc. J Appl Polym Sci 114: 3097–3105, 2009

Key words: composites; mechanical properties; microstructure; poly(propylene) (PP); structure-property relations

INTRODUCTION

For several decades, many studies have dealt with polypropylene (PP) filled with inorganic particles. From a general point of view, the mechanical properties of PP are modified in the presence of fillers, including talc,[1–6] calcium carbonate,[7–9] and clay.[10–12] Moreover, the polymer microstructure can also be affected by the fillers. For example, several authors have underlined the nucleating role of calcium carbonate modified by stearic acid, which promotes the stability of the β phase and/or increases the number of spherulites.[7,13] Talc has also been found to be a nucleating agent, and the relationships between the talc size and the induced microstructure of composites were studied by Ferrage et al.[6]

It is well known that the use of nanometric fillers can greatly modify the macroscopic properties of a polymer matrix. Indeed, a decrease in the filler size induces a decrease in the distance between two filler particles, which may be of the same order of magnitude as that of the crystalline lamella length. At the same time, when the specific area of the filler increases, the interface effects (the interfacial adhesion strength and fraction of the interphase) are amplified. Combined with the major role of the filler aspect ratio, all these advantages have led to numerous studies on polymer-based nanocomposites. Among those studies, many have focused on polymers filled with lamellar fillers such as clay. It has been shown that the macroscopic properties are governed by the orientation of the polymer crystalline lamellae and of the clay particles,[14,15] which is directly induced by the nanocomposite elaboration process.[16,17] This led to the proposal of an ideal microstructure for polymer/clay nanocomposites, which would include the formation of a rigid network[18] combined with high interfacial adhesion strength.[19] In the ideal microstructure, complete exfoliation of clay would not always be necessary, as suggested by Van Es.[20] It can also be noticed that the formation of such a network would be possible only if the mean distance between two clay particles and the typical length of a crystalline lamella were of the same order of magnitude.

Despite interesting properties, the weak points of clay can be identified. First, the enhancement of the

Correspondence to: K. Masenelli-Varlot (karine.masenelli-varlot@insa-lyon.fr).

macroscopic properties highly depends on the clay dispersion state. Although it is controlled in polyamide 6, with almost complete exfoliation, to the best of our knowledge, no solution has been found yet to correctly exfoliate clay in polyolefins (PP or polyethylene). From this point of view, it would be interesting to develop fillers that behave as clay but that do not have to be exfoliated.

In this article, we study the potentialities of submicrometer talc (μ-talc) as a filler for PP. PP filled with conventional micrometer-sized talc is also studied for comparison. The microstructure of the composites is first characterized in terms of the PP crystallinity [degree of crystallinity (X_c), phase, and orientation], μ-talc size distribution, and orientation. Then, the mechanical properties are presented and discussed as a function of the existence of a rigid network. Finally, the effect of the talc average thickness is presented.

EXPERIMENTAL

An isotactic PP (M_w = 380,000, IP ≈ 1.2) was obtained from Multibase (Dow Corning Co., Saint Laurent duPont, France). Two types of talc particles, namely μ-talc and conventional talc, were also obtained from Multibase.[21] The specific areas of the μ-talc and conventional talc, measured by the Brunauer–Emmett–Teller method, were 17 and 6.2 m^2/g, respectively. The average aspect ratios were 5.5 for μ-talc and 1.3 for conventional talc.

Benchmark studies were carried out with MPH3015T1 20541 from Multibase as a master batch (30 wt % μ-talc), which was diluted directly in virgin PP on a standard injection-molding press. The μ-talc fraction ranged from 3 to 30 wt %. The fraction of conventional talc was set to 3 or 20 wt %. Moreover, samples of pure PP were also elaborated. The characteristics of all the samples are summarized in Table I. After elaboration, the real talc fractions were determined by thermogravimetric analysis. It was found that they were very close to the nominal values. Thus, only the nominal values are used in the following discussion.

Differential scanning calorimetry (DSC) analyses were carried out on a DSC7 from PerkinElmer (Waltham, MA) under a nitrogen atmosphere with a heating/cooling rate of 10°C/min from 25 to 200°. Two heating cycles were realized to separate the influence of the processing conditions and of the clay on the polymer crystallization. Samples (10 mg) were cut in the middle of the injected sheets. X_c was calculated with the following law:

$$X_c = \frac{\Delta H_f}{\Delta H_f^o} \quad (1)$$

TABLE I
Materials

Name	Type of talc	Nominal talc fraction (wt %)	Real talc fraction (wt %)
PP	μ-Talc	0	0
PP-3	μ-Talc	3	2.7
PP-5	μ-Talc	5	5.2
PP-7	μ-Talc	7	6.4
PP-10	μ-Talc	10	10.6
PP-20	μ-Talc	20	19.2
PP-30	μ-Talc	30	28.9
PP-3c	Conventional talc	3	2.6
PP-20c	Conventional talc	20	19.8

The real talc fraction was determined by thermogravimetric analysis.

where ΔH_f is the specific melting enthalpy of the considered polymer and ΔH_f^o is the melting enthalpy of a 100% crystalline polymer at the temperature of the thermodynamic equilibrium (207 J/g for PP[22]). As far as the composites were concerned, eq. (1) was multiplied by a factor of $1/(1 - \phi)$, where ϕ is the talc ratio. The obtained X_c values were determined with an accuracy of ±0.5%.

The orientations of the PP crystalline lamellae and of the talc particles were determined from wide-angle X-ray scattering (WAXS) experiments at room temperature in the transmission mode with a Princeton (Trenton, NJ) SCX2D charge-coupled device camera. The X-ray beam was collimated with a point-focusing Göbel mirror from Xenocs (Sassenage, France) that ensured both monochromatized Cu Kα radiation (wavelength = 1.54 Å) and parallel point focusing. The samples, small cubes with a side length of about 2 mm, were taken from the middle of the injected sheets. Different sample-to-detector configurations were used (see Fig. 1). For that purpose, projections are designated with the principal sample axis denomination: Md for the machine direction (i.e., the injection direction), Td for the transverse direction, and Nd for the normal direction. The scattered vector varied between 0.6 and 6 nm^{-1}; it was obtained for an angular domain of $2\theta = 0.8°$ to $2\theta = 30°$. Two-dimensional (2D) scattering patterns were analyzed that took into account the transmission coefficient and the background diffusion with and without the X-ray beam.

The crystalline lamellae and talc orientations were quantified by a ternary diagram called the Wilchinsky diagram, the construction of which was detailed by Bafna et al.[23] In short, average squared cosines were calculated. These squared cosines, $\cos^2(\phi_{Nd})$, $\cos^2(\phi_{Td})$, and $\cos^2(\phi_{Md})$, were obtained from the Md–Nd and Md–Td patterns. The third projection, in the Td–Nd plane, allowed checking of the results. In practice, given values of **q*** [q value at maximum

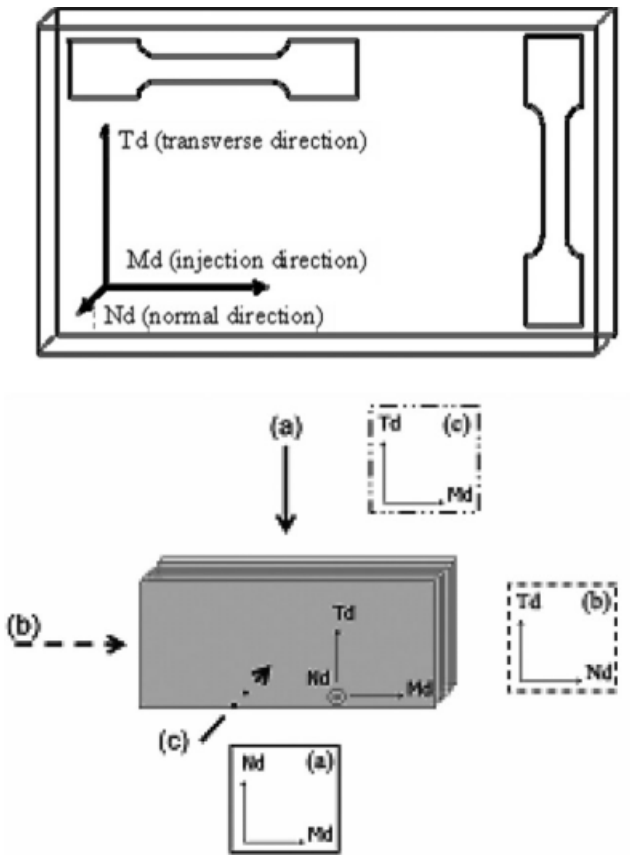

Figure 1 Different sample-to-detector configurations for the acquisition of 2D WAXS patterns.

intensity (for a given diffraction peak) in a Lorentz-corrected WAXS pattern of Iq^2 versus q] were chosen, which referred to the diffraction of particular (*hkl*) crystalline planes. The (002) and (040) planes at $\mathbf{q}^* \approx 5\ nm^{-1}$ and $\mathbf{q}^* \approx 10\ nm^{-1}$, respectively, were chosen for talc and PP, respectively. The corresponding points on the Wilchinsky diagram characterized the orientation of the normal to the planes in the Md, Nd, and Td frame. For a randomly oriented (*hkl*) plane, $\cos^2(\phi_{Md}) = \cos^2(\phi_{Td}) = \cos^2(\phi_{Nd}) = 1/3$, and the corresponding point is located in the center of the triangle. For a perfect orientation of the (*hkl*) plane parallel to the Md–Td plane, the corresponding point is located at the $\cos^2(\phi_{Nd})$ apex.

Scanning electron microscopy (SEM) observations were carried out on a JEOL (Tokyo, Japan) JSM-840A operating at 20 kV. The samples were cryofractured perpendicularly to the Md direction and coated with a thin layer of gold before observation. Several images were taken at random positions. Energy-dispersive spectrometry maps were sometimes recorded to distinguish the talc particles from the PP fracture surface. The thicknesses of the talc particles were measured with EsiVision software.

Tensile tests were performed on dumbbell-shaped specimens (30-mm gauge length and 4-mm width) at room temperature on an Instron (Norwood, MA) MTS1/ME machine with a crosshead speed of 2 mm/min. Young's modulus, the yield stress, the maximum stress, and the strain at break were determined.

Because the mechanical properties of the films might be anisotropic, tensile tests were carried out in two loading directions, Md and Td. For each material and loading direction, four samples were studied.

Compression tests were carried out on small cubes of composites (1.75-mm side length) on an Instron 8561 machine (two compression plates) in the three directions (Md, Td, and Nd). The compression speed was 0.1 mm/min. The cubes were thought to be small enough to prevent buckling and casklike deformation.

RESULTS AND DISCUSSION

PP/μ-talc composites

Microstructure

Figure 2 displays typical SEM images of PP-20 and PP-20c cryofractured surfaces. The talc particles appeared brighter than the PP matrix. They were obviously very well oriented in the injection plane (Md–Td), whatever the talc type. This preferential orientation was confirmed by WAXS. The thickness distributions of the talc particles in PP-20 and PP-20c were measured on 98 and 29 particles, respectively (see Fig. 2). The thickness distribution of μ-talc in PP-20 seemed to follow a log-normal distribution, with an average thickness of 0.39 μm and a standard deviation of 0.13 μm. μ-talc is thus considered a talc with submicrometer thicknesses. As far as conventional talc in PP-20c is concerned, the law of the thickness distribution would instead be Gaussian, although in this case the low number of measured talc particles probably led to strong uncertainties in the observed frequencies of each talc class. In this case, however, the measured average thickness was equal to 1.3 μm, and the standard deviation was equal to 0.4 μm. The measured average thickness confirmed that the conventional talc was composed of micrometer-sized talc particles. From SEM observations, it could also be seen that the fillers were well dispersed whatever the talc type and the talc fraction. This was due on the one hand to the use of a compatibilizer in the master batch and on the other hand to the extrusion conditions.

The main crystallinity characteristics of pure PP and PP in the PP/μ-talc composites were determined by DSC (see Fig. 3 and Table II). It is noteworthy that all the composites, filled with either μ-talc or conventional talc (not shown), exhibited the same behavior, which significantly differed from that of pure PP. Indeed, the crystallization temperature (T_c) increased from 117.6 to 125.6°C when 3 wt % μ-talc was incorporated. This confirms that talc acts as a

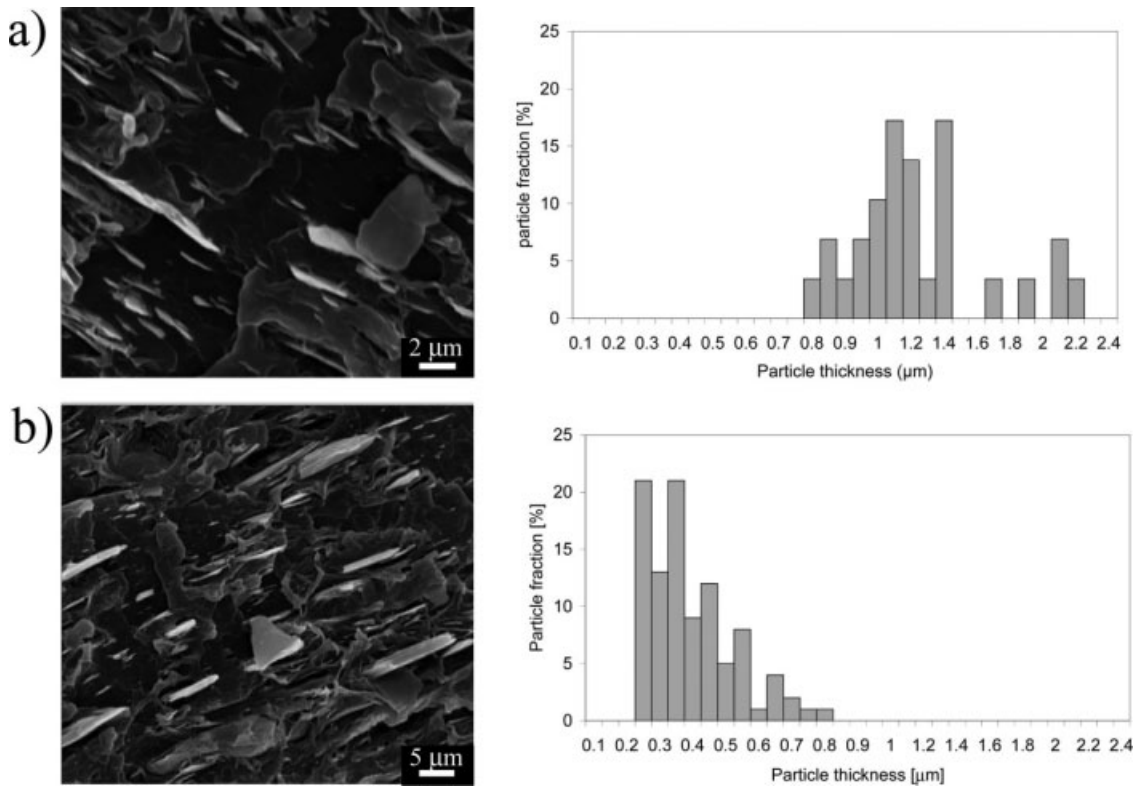

Figure 2 SEM images of cryofractured surfaces and measured size distributions of talc particles in (a) PP-20 and (b) PP-20c.

nucleating agent, as previously mentioned in the literature.[6,24] A slight increase was also observed when the µ-talc loading was further increased, but as this increase was moderate, the nucleation speed was considered constant whatever the talc type and talc loading. As far as the crystallite fusion temperature (T_f) is concerned, only one peak could be detected between 165.5 (PP) and 167.5°C (PP/µ-talc composites with talc loadings $\geq$5 wt %). This peak could be assigned to the fusion of PP crystallites in the α phase. No peak with respect to the β phase could be detected by DSC. Lastly, X_c of PP also

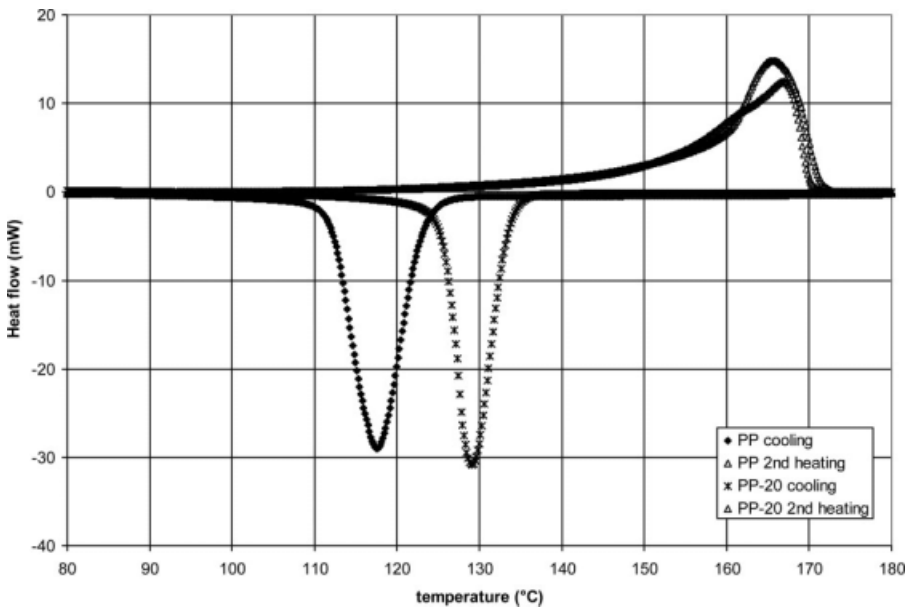

Figure 3 DSC thermograms of PP and PP-20 revealing the crystallization behavior and the crystallite fusion (second heating cycle).

TABLE II
T_c, T_f, and X_c Values of PP in Pure PP and in PP/μ-Talc Composites

Name	T_c (°C)	T_f (°C)	X_c (%)
PP	117.6	165.5	50.0
PP-3	125.6	166.5	52.5
PP-5	126.0	167.5	52.5
PP-7	126.5	167	52.5
PP-10	127.0	167.5	52.5
PP-20	129.5	167	53.0
PP-30	130.5	167	53.5

increased (from 50% to ca. 53%) when talc was incorporated, and then it did not significantly depend on the talc type or talc fraction.

The 2D WAXS patterns of PP-20, acquired in the three sample-to-detector configurations, are presented in Figure 4. The 2D WAXS patterns of the other materials studied (not displayed) were similar to those of PP-20. In direction a, all the peaks except for peak 1 ($2\theta = 9.5°$), which corresponded to the diffraction of the talc (002) planes, could be assigned to the PP α phase:[25] peaks 2, 3, 4, and 5 at 2θ values of 14.1, 16.9, 18.6, and 21.9° corresponded to the diffraction of the (110), (040), (130), and (−131) planes, respectively. No peak characteristic of the β phase could be detected (e.g., at $2\theta = 16.1$ or 21°). This is in agreement with the DSC results, from which it was concluded that the α phase could be considered the only existing phase.

Moreover, almost all the planes of the PP α phase gave rise to rings in direction c, but not in the other directions. At the same time, talc diffracted only along the Nd direction. This clearly indicates that a strong texture was created in the samples. Qualitatively, the diffraction of talc [(002) planes] only along the Nd direction indicates that talc particles lay in the plane of the sample, that is, the Md–Td plane. The orientation of the PP α-crystalline lamellae was not obvious because the peak of the (010) plane, parallel to the plane of the crystalline lamellae, could not be isolated in the spectra. The only qualitative information on the crystalline lamella orientation was given by the rings in direction c, which revealed an orthotropic orientation in the Md–Td plane.

The Wilchinsky diagram was used to quantify the preferential orientation of the talc particles and the PP crystalline lamellae. In Figure 5 are displayed the orientations of the vectors normal to the (002) and (040) planes in talc and PP, respectively. As far as talc is concerned, the vector normal to the (002) plane was parallel to the stacking direction. For all the samples, this vector was found to align in the Nd direction, and this means that the talc particles tended to lie in the plane of the injected samples (in an orthotropic way because the corresponding points were located on the bisector). This was previously observed with montmorillonite particles and was attributed to shear during the injection process.[20] Yet, although the montmorillonite platelets were always found to align almost perfectly in the injection plane, the orientation of the talc particles was better for high talc loadings (>10 wt % μ-talc). The difference between talc and clay might be attributed to their different aspect ratios. This could also well account for the observed difference in the orientation of talc in the composite containing 20 wt % conventional talc (PP-20c). Indeed, the orientation along the Nd direction was similar to that of talc in PP-7, which contained only 7 wt % μ-talc.

The orientation of the vector normal to the (040) planes in the crystalline lamellae of PP is also displayed in Figure 5. In pure PP, it was orthotropically

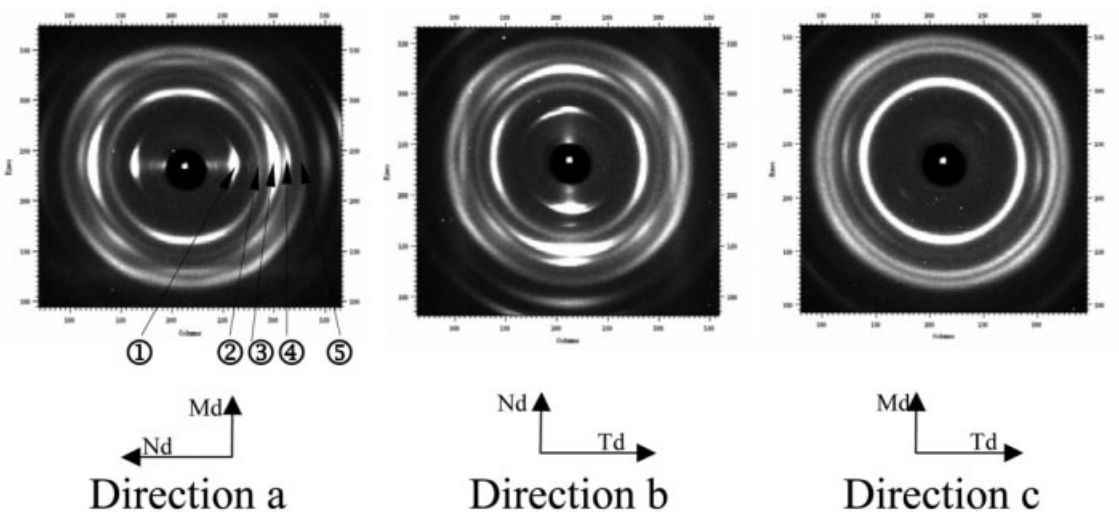

Figure 4 2D WAXS patterns of PP-20 acquired in the three sample-to-detector configurations defined in Figure 1.

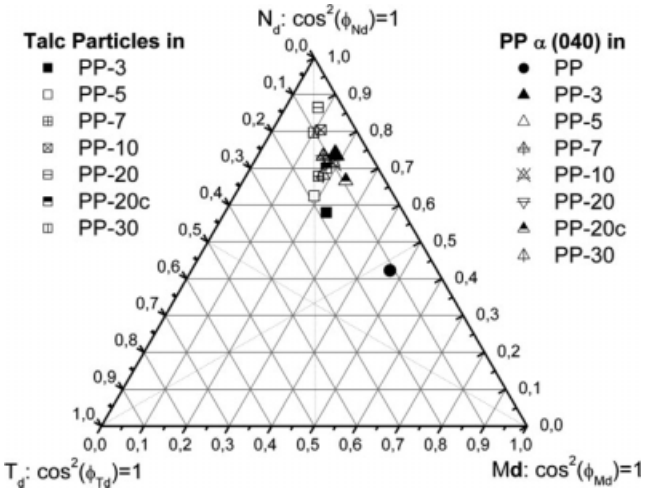

Figure 5 Wilchinsky diagram revealing the orientation of the normal vector to the (002) planes of talc and the orientation of the normal vector to the (040) plane of the PP crystalline lamellae.

distributed perpendicularly to the Td direction, whereas in all the composites, it was well oriented parallel to the Nd direction as the vectors normal to the talc (002) planes. Talc thus induced a preferential orientation of the PP crystalline lamellae, and this was not surprising because talc was found to be a nucleating agent. Interestingly, the PP (040) plane orientation seemed to depend neither on the talc fraction nor on the talc type (μ-talc or conventional talc).

As a conclusion to the microstructural characterization of the materials, a schematic representation of the composite architecture is provided in Figure 6. It could indeed be concluded that the talc particles lay in the plane of the sample (Md–Td plane). In contrast to that of the talc particles, the orientation of the PP crystalline lamellae could not be directly deduced from the orientation of the plane used for quantifying the WAXS patterns. Indeed, the chain axis is represented by vector **c**. When we consider that vector **b**, perpendicular to the (040) planes, is perfectly oriented along the Nd direction and that the crystalline lamella orientation is orthotropic [as deduced from Fig. 4(c)], vector **c** is perpendicular to the Nd direction and orthotropically distributed in the Md–Td plane. This means that the crystalline lamellae are perpendicular to the talc particles without further orientation, as schematically drawn in Figure 6. Although no information was found on the talc–crystalline lamella interaction, the concept of networks will be used in the following discussion because of the talc nucleating behavior.

Mechanical properties

Figure 7 display the tensile curves obtained for pure PP and for PP-20, the load direction being parallel to either Md or Td. For the other composites, the global shapes of the tensile curves are similar to the ones presented in Figure 7. Obviously, the materials exhibited similar tensile behaviors in both directions. In the composites, this result was expected from the microstructural characterization. In the case of pure PP, the tensile behavior did not depend on the load direction (Md or Td). This is in agreement with the microstructural characterization: even though in this case the orientation of the vector perpendicular to the PP crystalline lamellae could not be easily deduced from the orientation of vector **b**, an orthotropic orientation was noticed in the Md–Td plane.

Young's moduli of the composites can be represented as a function of the μ-talc fraction (see Fig. 8). For all the materials, no significant difference was observed between Md and Td, as expected. From the schematic microstructure (Fig. 6), the easiest model for describing the evolution of Young's modulus is the law of mixtures (parallel coupling), with talc particles and a homogeneous PP matrix in parallel. Young's modulus of PP was set to 1.7 GPa, as experimentally measured on the pure PP samples. Young's modulus of talc (28.2 GPa), obtained after least square minimization, was far smaller that that proposed in the literature,[26] probably because the value given in the literature was obtained on randomly oriented talc, whereas the talc particles were well aligned in the composites studied here. Between 3 and 10 wt % μ-talc, the measured values of Young's modulus were higher than those calculated. It could be deduced that a percolating PP/talc network started to form below 3 wt % and was completely formed around 10 wt %. Indeed, far below 3 wt %, the distance between two adjacent talc particles was too large to permit their connection by PP crystalline lamellae. When the talc fraction was increased, the distance decreased, and for a critical talc fraction, one crystalline lamella could bridge two adjacent talc particles. The formation of such a

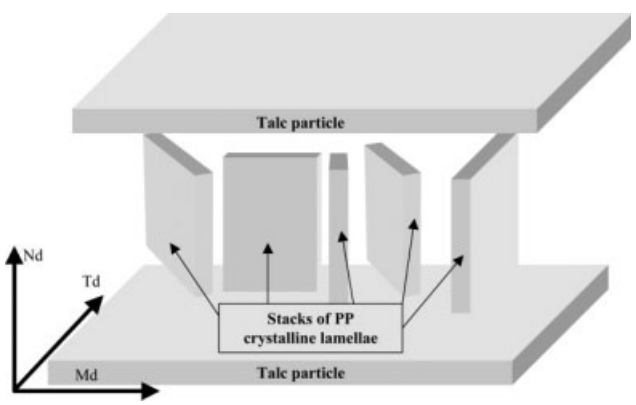

Figure 6 Schematic description of the composite microstructure with the orientations of the talc particles and the PP crystalline lamellae.

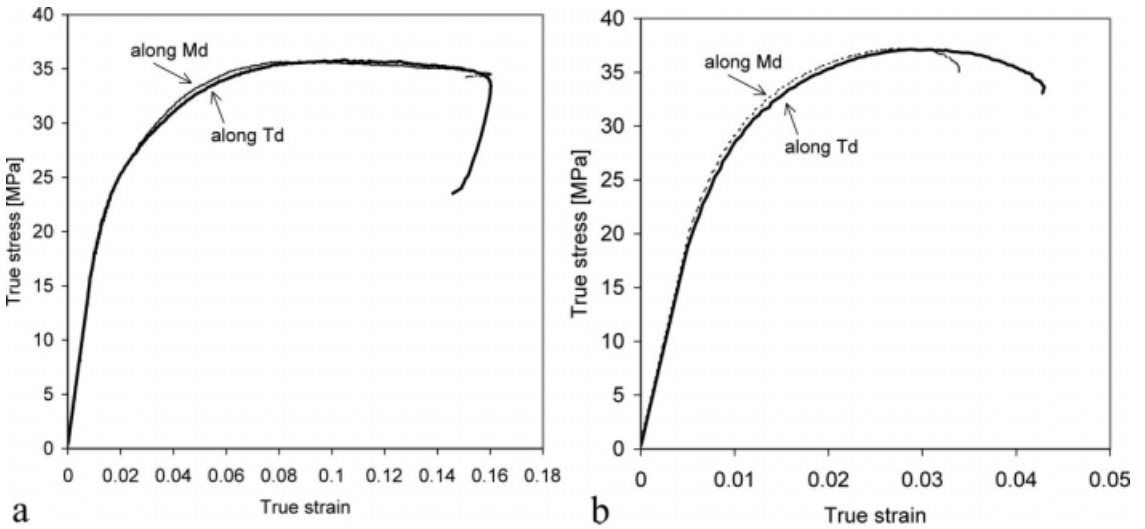

Figure 7 Tensile curves of (a) pure PP and (b) PP-20, the load direction being parallel to either Md or Td.

network and the existence of a critical filler fraction were previously proposed as ideal microstructures for improved mechanical properties of polymer/clay nanocomposites.[19] However, the value of the critical filler fraction could not be measured in polymer/clay nanocomposites, most likely because the clay exfoliation state might depend on the clay fraction. In our case, and from a simple geometrical model, the distance between two μ-talc particles could be estimated to be 39 μm in PP-3 (which contained 1 vol % μ-talc, each μ-talc particle having a thickness equal to the average thickness measured, 0.39 μm). This distance was of the same order of magnitude as that of a crystalline lamella length, and it can thus be concluded that the mixed percolating threshold could be formed with a 3 wt % μ-talc loading.

Interestingly, for talc fractions higher than 10 wt %, the reinforcement can be well described by the parallel law of mixtures. It is proposed that once the percolating network is formed, the incorporation of talc particles does not significantly modify this network and induces classical reinforcement.

A similar conclusion can be drawn from the variations of the yield stress (see Fig. 9) and strain at break (not displayed). With 3 wt % μ-talc, the yield stress sensitively increased, whereas the strain at break decreased. Between 3 and 10 wt % μ-talc, that is, during the formation of the percolating network, no significant variation could be observed. For higher μ-talc loadings, both the yield stress and the strain at break decreased in a moderate way. As far as the tensile properties are concerned, it can thus be concluded that the formation of the percolating

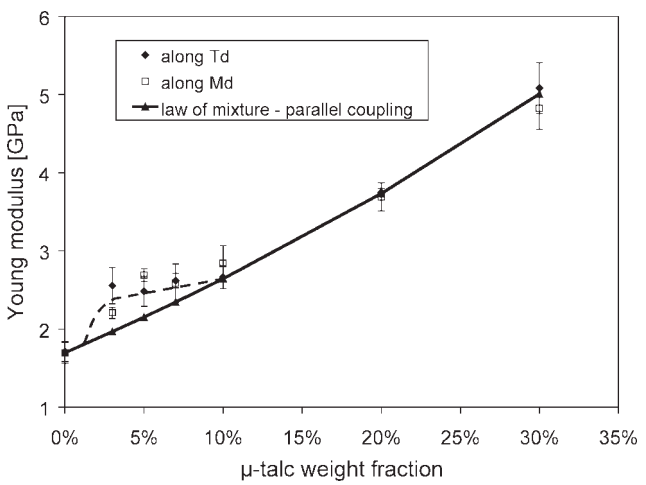

Figure 8 Young's modulus of the PP/μ-talc composites as a function of the μ-talc fraction. Values calculated with the law of mixtures are given for comparison.

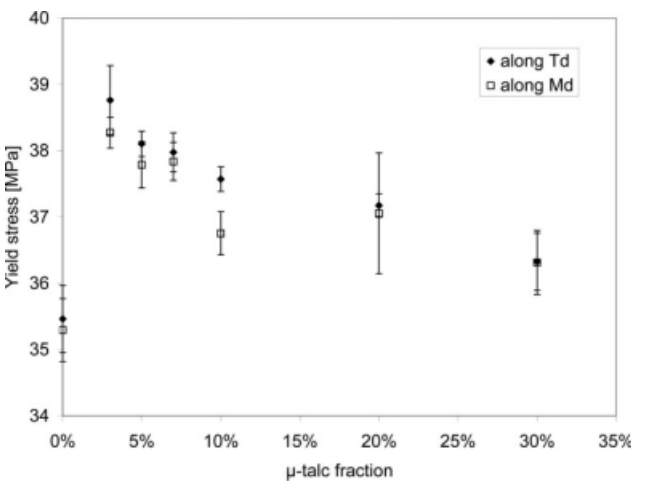

Figure 9 Yield stress of the PP/μ-talc composites as a function of the μ-talc fraction.

network plays a major role. The optimum μ-talc fraction is between 3 and 10 wt %.

From the observed microstructure (Fig. 6), the mechanical behavior was expected to be different when the loading direction was along Nd. Unfortunately, this load direction could not be characterized by tensile tests. Compression tests were thus carried out along the three directions (Md, Td, and Nd). The compression curves are displayed in Figure 10 for PP-20. The compression curves of all the PP/μ-talc composites are similar. In agreement with the observed microstructure and with the tensile tests, it can be observed that the composites exhibited the same mechanical behavior in the Md and Td directions, whereas the yield stress was higher in the Nd direction.

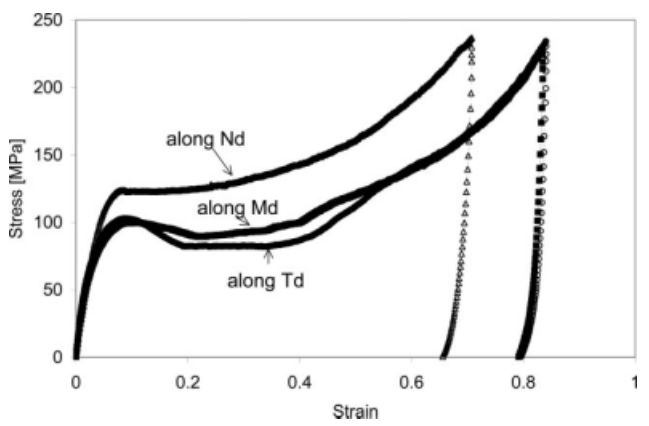

Figure 10 Compression curves of PP-20, the load direction being parallel to Md, Td, or Nd.

Effect of the talc size

To study the effect of the talc thickness, tensile tests were also carried out on PP-3c and PP-20c, which contained 3 and 20 wt % conventional talc, respectively. Young's modulus was measured in the Td direction. The reinforcement was significantly higher in PP-3 than in PP-3c: in comparison with pure PP, the increases in the modulus were 30 and 10%, respectively, whereas PP-20 and PP-20c exhibited similar reinforcements. It has to be recalled that in PP-3, a percolating network was being formed. The formation of the networks started at a critical talc fraction, at which the distance between two adjacent talc particles became comparable to the length of the PP crystalline lamellae. Hence, the critical talc fraction was highly dependent on the talc mean thickness. The weakest reinforcement in PP-3c therefore suggested that the critical talc fraction was not attained. The standard talc fraction, which led to a mixed percolating network similar to that obtained with 3 wt % μ-talc, could be estimated with a geometrical model. Indeed, a distance of 39 μm between two talc particles corresponded to 3 vol % talc, that is, 8.5 wt %. From that point of view, it became obvious that with 3 wt % standard talc, the percolating threshold was not reached.

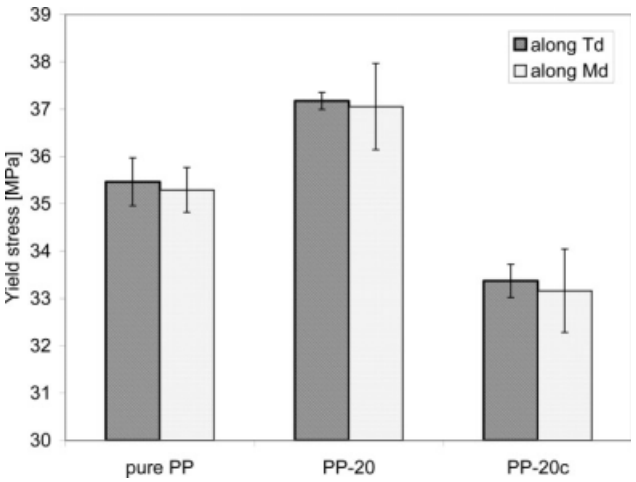

Figure 11 Comparison of the yield stresses of PP, PP-20, and PP-20c.

With 20 wt % talc, the reinforcements were similar. This highlights the fact that once the percolating network has been formed, the reinforcement can be well described by a law of mixtures: in that model, the filler size is not taken into account. Interestingly, although PP-20 and PP-20c exhibited the same Young's modulus, their yield stresses were different. The yield stress of PP-20 was significantly higher than that of PP-20c. Moreover, it was higher than that of pure PP, whereas that of PP-20c was lower (Fig. 11).

CONCLUSIONS

The microstructure and mechanical properties of injected PP/talc composites were studied. Two different types of talc were used, namely, conventional micrometer-sized talc and submicrometer talc (μ-talc). The thickness distributions of the talc particles in the composites were determined from SEM images.

The microstructural characterization led to a schematic description of the composite microstructure, with the talc particles lying in the plane of the injected samples and the PP crystalline lamellae being perpendicular to the talc particles (in an orthotropic way, i.e., without any further orientation). Consequently, the mechanical properties in plane were also found to be orthotropic, whereas a significant reinforcement was found out of plane.

The composite microstructure revealed the existence of a mixed talc/crystalline lamella network, and the network formation was followed with tensile tests at different talc fractions. Indeed, the reinforcement was higher than expected from a parallel

law of mixtures for μ-talc loadings ranging from 3 to 10 wt %. This deviation was attributed to the network percolation. Once the network was completely formed (i.e., for μ-talc loadings >10 wt %), the reinforcement could be well described by the law of mixtures. A μ-talc concentration of 3–10 wt % seemed to be the optimum talc loading, with a reinforcement higher than expected combined with a large increase in the yield stress.

Moreover, the talc fraction at which percolation occurred was found to be highly dependent on the average talc thickness: obviously, 3 wt % conventional talc did not permit this threshold to be reached, and the reinforcement was lower than that obtained with μ-talc. After completion of the network, the classical variations of Young's modulus induced similar reinforcements, whatever the type of talc. Yet, differences remained in the yield stress.

This study confirms the interest in fillers of reduced thickness. From a general point of view, although it is not classified as a nanofiller, μ-talc may be a good compromise because its thickness is in the submicrometer range, it can quite easily be functionalized, and it does not exfoliate during incorporation into the polymer matrix.

The authors thank P. Prèle and Multibase-Dow Corning for kindly providing the materials.

References

1. Velasco, J. I.; Desaja, J. A.; Martinez, A. B. J Appl Polym Sci 1996, 61, 125.
2. Qiu, W.; Mai, K.; Zeng, H. J Appl Polym Sci 2000, 77, 2974.
3. Naiki, M.; Fukui, Y.; Matsumura, T.; Nomura, T.; Matsuda, M. J Appl Polym Sci 2001, 79, 1693.
4. Naguib, H.; Park, C. B.; Lee, P. C. J Cell Plast 2003, 39, 549.
5. Mucha, M.; Królikowski, Z. J Therm Anal Calorim 2003, 74, 549.
6. Ferrage, E.; Martin, F.; Boudet, A.; Petit, S.; Fourty, G.; Jouffrey, F.; Micoud, P.; De Parseval, P.; Salvi, S.; Bourgerette, C.; Ferret, J.; Saint-Gérard, Y.; Buratto, S.; Fortune, J. P. J Mater Sci 2002, 37, 1561.
7. Labour, T.; Gauthier, C.; Séguéla, R.; Vigier, G.; Bomal, Y.; Orange, G. Polymer 2001, 42, 7127.
8. Zuiderduin, W. C. J.; Westzaan, C.; Huétink, J.; Gaymans, R. J. Polymer 2003, 44, 261.
9. Thio, Y. S.; Argon, A. S.; Cohen, R. E.; Weinberg, M. Polymer 2002, 43, 3661.
10. Solomon, M. J.; Almusallam, A. S.; Seefeldt, K. F.; Somwangthanaroj, A.; Varadan, P. Macromolecules 2001, 34, 1864.
11. Chrissafis, K.; Paraskevopoulas, K. M.; Stavrev, S. Y.; Doscoslis, A.; Vassiliou, A.; Bikiaris, D. N. Thermochim Acta 2007, 465, 6.
12. Liu, X.; Wu, Q. Polymer 2001, 42, 10013.
13. Chan, C.-M.; Wu, J.; Li, J.-L.; Cheung, Y.-K. Polymer 2002, 43, 2981.
14. Varlot, K.; Reynaud, E.; Klopper, M. H.; Vigier, G.; Varlet, J. J Polym Sci Part B: Polym Phys 2001, 39, 1360.
15. Masenelli-Varlot, K.; Reynaud, E.; Vigier, G.; Varlet, J. J Polym Sci Part B: Polym Phys 2002, 40, 272.
16. Velasco, J. I.; Morhain, C.; Martineza, A. B.; Rodriguez-Pérez, M. A.; de Saja, J. A. Polymer 2002, 43, 6805.
17. Choi, W. J.; Kim, S. C. Polymer 2004, 45, 2393.
18. Kim, G. M.; Lee, D. H.; Hollmann, B.; Kressler, J.; Stöppelmann, G. Polymer 2001, 42, 1095.
19. Masenelli-Varlot, K.; Vigier, G.; Vermogen, A.; Sixou, B.; Gauthier, C.; Cavaillé, J. Y. J Polym Sci Part B: Polym Phys 2007, 45, 1243.
20. van Es, M. Ph.D. Thesis, Technische Universiteit Delft, 2001.
21. Prèle, P.; von Tschammer, A.; Crépin-Leblond, J. Presented at the World Automotive Congress, Rome, Italy, 2007.
22. Zhou, X.-P.; Xie, X.-L.; Yu, Z.-Z.; Mai, Y.-W. Polymer 2007, 48, 3555.
23. Bafna, A.; Beaucage, G.; Mirabella, F.; Mehta, S. Polymer 2003, 44, 1103.
24. de Medeiros, E. S. J Therm Anal Calorim 2001, 66, 523.
25. Natta, G.; Corradini, P. Nuovo Cimento 1960, 15, 40.
26. Martinatti, F.; Ricco, T. J Mater Sci 1994, 29, 442.